Diamond & Related Materials 19 (2010) 1446–1452

Contents lists available at ScienceDirect

Diamond & Related Materials

journal homepage: www.elsevier.com/locate/diamond

Improved microwave plasma cavity reactor for diamond synthesis at high-pressure and high power density

K.W. Hemawan [a], T.A. Grotjohn [a], D.K. Reinhard [a], J. Asmussen [a,b,*]

[a] Dept. of Electrical & Computer Engineering, 2120 Engineering Building, Michigan State University, East Lansing, MI, 48824 USA
[b] Fraunhofer Center for Coatings and Lasers Applications, B100 Engineering Research Complex, Michigan State University, East Lansing, MI, 48824 USA

ARTICLE INFO

Article history:
Received 12 November 2009
Received in revised form 17 June 2010
Accepted 31 July 2010
Available online 14 August 2010

Keywords:
Microwave plasma CVD
Reactor design
Diamond synthesis
Enhanced growth

ABSTRACT

Microwave plasma assisted synthesis of diamond is experimentally investigated using high purity, 2–5% CH_4/H_2 input gas chemistries and operating at high pressures of 180–240 Torr. A microwave cavity plasma reactor (MCPR) was specifically modified to be experimentally adjustable and to enable operation with high input microwave plasma absorbed power densities within the high-pressure regime. The modified reactor produced intense microwave discharges with variable absorbed power densities of 150–475 W/cm^3 and allowed the control of the discharge position, size, and shape thereby enabling process optimization. Uniform polycrystalline diamond films were synthesized on 2.54 cm diameter silicon substrates at substrate temperatures of 950–1150 °C. Thick, freestanding diamond films were synthesized and optical measurements indicated that high, optical-quality diamond films were produced. The deposition rates varied between 3 and 21 μm/h and increased as the operating pressure and the methane concentrations increased and were two to three times higher than deposition rates achieved with the MCPR operating with equivalent input methane concentrations and at lower pressures (≤140 Torr) and power densities.

1. Introduction

It is now widely recognized [1–8] that chemical vapor deposition (CVD) diamond growth rates can be increased by carrying out synthesis above 100 Torr and by using high power density microwave discharges. It is now further speculated that by increasing the deposition pressure beyond 180 Torr and by increasing the discharge power density, the diamond growth rates can be increased considerably while still yielding good quality diamond. Thus, research groups [7–16] are exploring new reactor designs and new process methods for higher pressure (>150 Torr) and higher power density (>150 W/cm^3) microwave plasma assisted chemical vapor deposition (MPACVD) diamond synthesis. In particular, Ref. [14] provides a summary of the state-of-the-art of MPACVD reactor technologies and also notes the potential for increased diamond synthesis rates and improved diamond quality under high-pressure and high power density operation. Thus, the goal of this investigation is to further explore, develop and extend MPACVD reactor technologies to higher pressures thereby enabling high deposition rate processes that rapidly synthesize high quality diamond.

Here, we report the results of an exploratory investigation that had the objective of experimentally evaluating polycrystalline diamond (PCD) MPACVD diamond synthesis at pressures of 180–240 Torr and at high discharge power densities (>150 W/cm^3). The experiments employ a specific reactor geometry [3,18] identified here as the microwave cavity plasma reactor (MCPR). As was reported earlier [3,17–19], when operated in the 100–160 Torr pressure regime this reactor has synthesized high quality and high growth rate CVD polycrystalline diamond material. In this investigation, the MCPR is first modified to operate with high power densities at pressures above 180 Torr. Then the performance of this modified reactor is experimentally explored over the 180–240 Torr pressure regime by synthesizing PCD diamond. In particular, the following data and results are presented for the high-pressure operating regime: (1) the experimentally measured absorbed discharge power density and the associated deposition rates versus pressure, methane concentration and reactor tuning, (2) the importance of physically tuning the reactor in order to achieve high deposition rates and optimal spatial uniformity over one inch substrates, and (3) the ability to synthesize optical-quality PCD film within this high-pressure (180–240 Torr) regime. The experimental performance is compared with the performance of a similar reactor [3,17–19] operating at lower pressures and lower discharge power densities.

2. Experimental reactor

A cross sectional view of a generic version of the MCPR is displayed in Fig. 1(a). The electromagnetic excitation region consists of a cylindrical waveguide (z>0) and a coaxial waveguide section (z<0). The substrate is placed on a molybdenum holder of radius R4 which is

* Corresponding author. Dept. Of Electrical & Computer Engineering, 2120 Engineering Building, Michigan State University, East Lansing, MI, 48824 USA.
E-mail address: asmussen@egr.msu.edu (J. Asmussen).

0925-9635/$ – see front matter © 2010 Elsevier B.V. All rights reserved.
doi:10.1016/j.diamond.2010.07.005

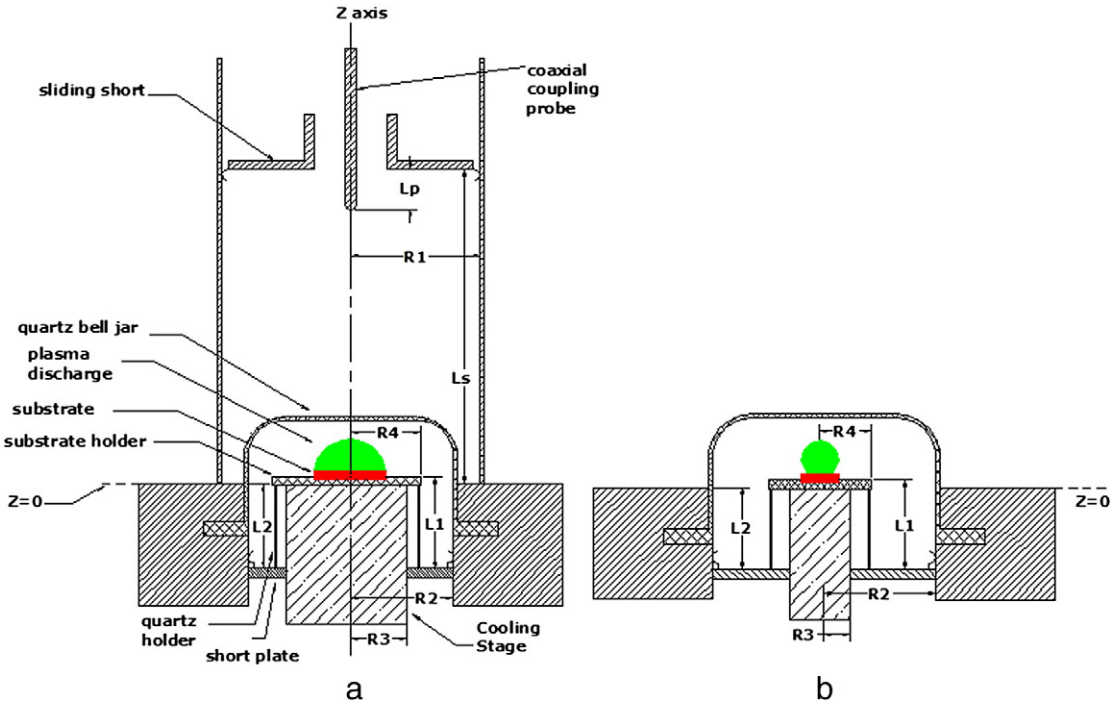

Fig. 1. (a) Cross sectional view of the reference reactor. (b) Modified substrate holder with reduced inner conductor (cooling stage) radius. The z = 0 plane separates the cylindrical and coaxial sections of the reactor.

in good thermal contact with the water-cooled stage of radius R3. The thickness of the molybdenum holder and the cooling rate are adjusted to achieve useful deposition substrate temperatures within the desired operating pressure regime. The reactor geometry is a function of the following geometric variables Ls, Lp, L1, L2, R1, R2, R3, and R4. Earlier experimental investigations used a 2.45 GHz MCPR design and explored CVD diamond synthesis over the low to moderate 60–160 Torr synthesis pressure regime. These results have been reported in several publications [3,17–20]. The specific dimensions of this reactor were R1 = 8.89 cm, R2 = 7.04 cm, R3 = 4.13 cm and R4 = 5.08 cm. These dimensions were chosen to enable diamond synthesis over 2–4 inch substrate areas when operating in the low to moderate pressure regime, i.e. this reactor was especially designed for operation at pressures of 20–160 Torr and to deposit diamond over modest to large area substrates. In this paper, we refer to this reactor as the "reference reactor" and we compare its experimental performance to the performance of the reactor design presented below.

In this investigation, we modified the MCPR reference reactor design to allow operation at higher discharge power densities and higher pressures. The redesign involved (1) adjusting the molybdenum substrate holder thickness and cooling rate to achieve the appropriate substrate deposition temperatures at the higher operating pressures and higher power densities, (2) reducing the substrate holder and inner conductor cooling stage radii, R4 and R3, as shown in Fig. 1(b), and (3) allowing the substrate holder stage to be tunable, i.e. allowing L1 and L2 to be variable. The specific redesign reported here reduced the substrate holder radius R4 to 3.24 cm and the inner conductor cooling stage radius R3 was reduced to 1.91 cm, i.e. the inner conductor area was reduced by about 4.5. This modification focuses the electromagnetic energy on the reduced diameter substrate holder and increases the axial electric field intensity and the associated electromagnetic displacement current density at the location of the substrate surface.

The reactor cylindrical/coaxial waveguide configuration allows the reactor to be excited in a hybrid, $TM_{013} + TEM_{001}$ electromagnetic mode. In order to achieve the hybrid excitation the top (z>0) cylindrical section length Ls is adjusted to be very close to $3\lambda_g/2$ where λ_g is the guided electromagnetic wavelength of the TM_{01} cylindrical waveguide mode and the coaxial section (z<0) length L2 is adjusted to approximately $\lambda_0/2$ where λ_0 is the free space wavelength at the 2.45 GHz excitation frequency. When properly adjusted, the top (z>0) cylindrical section is excited in the TM_{013} mode, and the lower (z<0) coaxial section is excited in the TEM_{001} mode. At the vicinity of the abrupt discontinuity plane, i.e. around z = 0, the total electric field is the sum of the TM_{013} field, the TEM_{001} field and the evanescent field that is induced by the "waveguide discontinuity" at the z = 0 plane. Thus, the electromagnetic field focus at and above the substrate (around the z = 0 plane) can be controlled and varied during experimental process development by length tuning L1 and L2. When a discharge is present, this length tuning varies the electromagnetic field focus above and around the substrate and within the discharge, and in turn, changes and controls the location, the shape and the absorbed power density of the discharge. There are some similarities between the reactor design presented here and the "evolved" Gicquel reactor design that is presented in Fig. 21 of Ref. [14]. A major difference however is the tunability of our reactor, especially the variation of L1, L2 around the z = 0 plane that enables process control and optimization.

In the experiments presented here Ls and Lp are adjusted to excite and match the TM_{013} mode in the cylindrical section of the applicator; i.e. Ls = 20.3 cm and Lp = 3.6 cm. During process optimization, L1 is held constant at 5.65 cm while L2 is varied between 5.16 cm and 6.13 cm and thus the position of the substrate holder defined as Zs = L1–L2, varies approximately between + 0.5 cm to about − 0.5 cm around the z = 0 plane.

3. Reactor operation and discharge characteristics

3.1. Plasma discharge behavior and reactor roadmap

Before plasma ignition, the reactor is length adjusted to excite the hybrid electromagnetic resonance. Discharge ignition is achieved at pressures of 5 Torr. Once the discharge is ignited, Ls and Lp are then

readjusted to match the microwave power into the applicator and hence into the discharge, and pressure is also increased to the desired operating pressure. The substrates were 25.4 mm diameter and 1.5 mm thick N-type silicon wafers. Each silicon wafer was nucleation seeded by mechanical polishing using natural diamond power of size ≤0.25 μm and cleaned using acetone and deionized water and then placed on the molybdenum holder. The linear diamond growth rates were determined by measuring the weight of the substrate before and after deposition (total weight gain) divided by the deposited substrate area and mass density of diamond 3.515 g/cm^3. Calibrated incident and reflected power meters were located in the input microwave circuit and the input absorbed microwave power was measured as the difference between the incident and reflected power.

The experimental pressure variation ranged between 180 and 240 Torr and microwave input powers varied between 1.8 and 2.4 kW. The reflected power was always less than 5% of the incident power, which indicated a good impedance match into the MCPR. Hydrogen and methane were the synthesis gases and the percentage of methane was varied from 2 to 5%. The hydrogen flow rate was fixed at 400 sccm and methane flow varied from 8 to 20 sccm. The H_2 and CH_4 input gases had purity levels of 99.9995% and 99.999% respectively and no additional N_2 was added into the gas system. A one-color pyrometer with emissivity set to 0.6 was used to monitor the substrate temperature through a viewing port window in the MCPR during the diamond deposition process.

After ignition at about 5 Torr, the plasma discharge initially filled the whole discharge chamber. As the pressure was gradually increased the plasma size began to shrink at about 60 Torr and became smaller as the pressure increased. At high pressure the discharge had a green color with an intense almost white center core. Fig. 2 displays the photographs of the discharge hovering over the silicon substrate as the operating pressure is increased from 180 to 260 Torr. As shown in the photographs, when the pressure increases the radius of the bright central core of the discharge becomes smaller than the deposition substrate area and yet the temperature across the diameter is uniform and the resulting diamond deposition is also uniform. This observation supports the results from recent CVD diamond synthesis modeling investigations [21,22] which have indicated that high concentrations of important diamond synthesis species occur outside the intense central discharge core.

When the reactor geometry, substrate size, methane concentration and total gas flow rate are held fixed the deposition process is a function of input power, pressure, and substrate temperature. The relationship between these variables is nonlinear and it can best be described by a set of experimental curves [17,20]. Fig. 3 displays such a set of curves for the redesigned reactor where the reactor cooling is constant, the reactor geometry is held fixed at Ls = 20.5 cm, Lp = 3.5 cm, and L2 = 6.13 cm, the total gas flow rate is 412 sccm, and the methane percentage and Zs were held fixed at 3% and −0.31 cm respectively.

Each of the experimental curves in Fig. 3 is plotted for a constant pressure and the set of curves displays the variation of the substrate temperature versus input microwave power over the entire 60–240 Torr pressure regime. In Fig. 3, the safe and process useful operating regime is the area enclosed within the dashed line boundary, i.e. the enclosed region displays the acceptable experimental operating region for process operation and optimization. The left hand side of the enclosed parallelogram is determined by the minimum power required to generate a discharge of sufficient size to cover the substrate while the right side of the parallelogram is determined by the power required to completely cover the substrate without touching the discharge chamber walls. Thus, at each operating pressure the right hand side of the data points represents the approximate limit of the maximum input power at that pressure before reactor wall heating becomes a problem and the left hand side determines the minimum amount of input power required to uniformly cover a 2.54 cm diameter substrate with diamond.

As can be observed in Fig. 3, as the pressure and input power increase the substrate temperature increases. At low pressures, the substrate temperature is more sensitive to pressure changes than at high pressures. However at low pressures, the change in substrate temperature is less sensitive to input power changes than at high pressure; i.e. the slope of the constant pressure curves increases as pressure increases. Thus when operating at high pressures, the experimental synthesis becomes sensitive to input power variations.

3.2. Discharge absorbed power density and substrate temperature

The experimental average discharge power density is defined as the input absorbed microwave power divided by the plasma volume. The plasma volume was approximated by taking size calibrated photographs of the discharge within the allowable reactor operating region, defining the discharge volume as the volume of the brightest luminescence of the discharge (i.e. the white central discharge core), and then determining the discharge volume from the visual photographs. An example of the experimentally measured discharge power density versus pressure for the modified high-pressure reactor is presented in Fig. 4. Here the experimental data for the redesigned reactor (the + data points) were taken with fixed reactor geometry where L2 was held constant at 6.13 cm (Zs = −0.48 cm) as the pressure is increased from 60 Torr to 240 Torr. As shown, the discharge power density increases from about 80 W/cm^3 to about 475 W/cm^3 as the pressure increases from 60 Torr to 240 Torr.

In Fig. 4, the redesigned reactor experimental power densities are also compared with the power densities of the reference reactor (the Δ data points). The power densities of the redesigned reactor are much larger than similar power densities from the reference reactor. Specifically, the corresponding absorbed power densities for the reference reactor shown in Fig. 4 vary from 20 to 45 W/cm^3 as the pressure increases from 80 to 140 Torr [3] while the corresponding discharge power densities of the redesigned reactor vary from 80 to 225 W/cm^3. The reduction of the center conductor area by about 4.5 increased the measured power density by a factor 4–5. Thus the increase in power density is inversely proportional to the substrate area and for a constant pressure the reduction of the substrate diameter significantly increases the power density of the discharge.

When operating at a constant pressure within the allowable deposition region shown in Fig. 3 the discharge power density and substrate temperature can be further varied and optimized by length tuning the coaxial cavity section. Thus, within the allowable

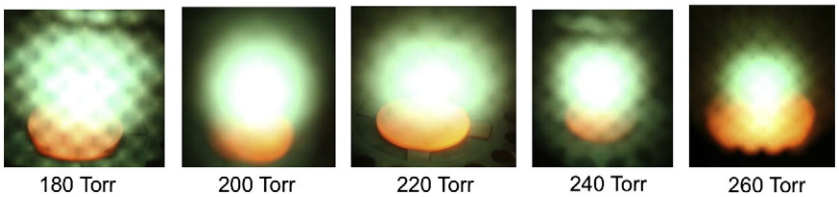

Fig. 2. Photographs of the discharge over the silicon substrate as the operating pressure is increased from 180 to 260 Torr. The microwave absorbed power ranges from 2.0 to 2.5 kW as pressure increases.

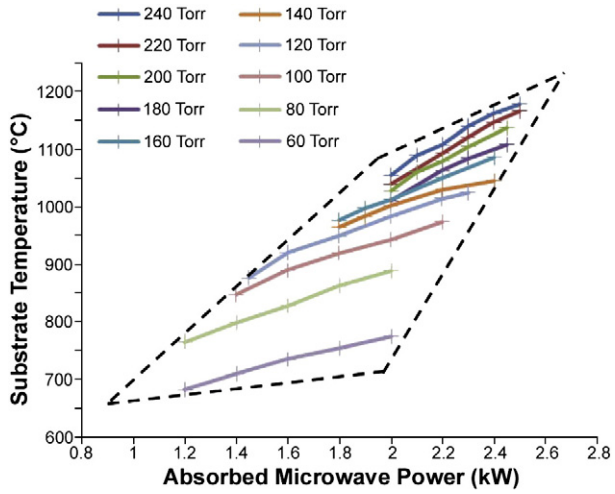

Fig. 3. The operating roadmap of the improved plasma reactor showing the substrate temperature versus absorbed microwave power at various operating pressures. Ls = 20.5 cm, Lp = 3.5 cm, L2 = 6.13 cm, H_2 = 400 sccm, CH_4 = 3%, and Zs = −0.31 cm.

deposition region shown in Fig. 3, each curve can be modified by adjusting the coaxial cavity section of the applicator. When this is done, the electromagnetic focus is altered around the z = 0 region and the substrate also is moved changing its axial position from above to the below the z = 0 plane. As the substrate position changes the position, size, shape and power density of the microwave discharge are also varied in a complex nonlinear fashion.

In particular, Figs. 4 and 5 display the variations of discharge power density and substrate temperature versus pressure as the substrate position is varied from above to below the z = 0 plane, i.e. Zs varies from +4.9 mm to −4.8 mm. These curves demonstrate that at a constant pressure, the substrate temperature can vary more than 300 °C and the associated plasma power density at 240 Torr also changes dramatically. For example as shown in Fig. 5, at 240 Torr as the substrate position is varied from +4.9 mm to −4.8 mm, the substrate temperature changes from 875 °C to 1175 °C. The substrate temperature increases as the substrate is lowered below the z = 0 plane. The associated discharge power densities, which are shown in Fig. 4, vary from about 225 W/cm^3 at Zs = +4.9 mm to 475 W/cm^3 at Zs = −4.8 mm. These experiments clearly demonstrate the ability to alter the substrate temperature and the discharge position and power density as the coaxial waveguide length is changed. As the substrate position is lowered from a position above to a position below the z = 0 plane the discharge position with respect to the substrate changes, the discharge volume decreases, the power density increases and the discharge becomes more intense, and the substrate temperature increases.

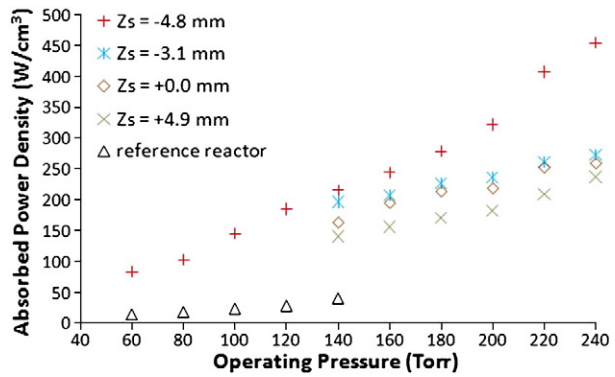

Fig. 4. The absorbed plasma power density with increasing pressure of the modified reactor at various Zs positions.

3.3. Reactor process optimization

At each operating pressure diamond synthesis was optimized by length tuning the coaxial section, i.e. a set of separate eight-hour deposition experiments were performed that explored the deposition rate and substrate temperature variation versus substrate position Zs. An example of such an optimization process is displayed in Fig. 6. In these experiments the pressure and methane concentration were held constant at 220 Torr and 3%, respectively. L1 was also held constant while L2 was varied in five steps as the substrate position varied from +4.9 mm to −4.9 mm. For each of the experimental data points presented in the figure, the discharge size was slightly adjusted by varying the input power a small amount around 2.4 kW to achieve uniform deposition. A uniform temperature distribution over the wafer was achieved by adjusting the reactor so that the plasma hovered around and remained in good contact with the substrate.

As shown in Fig. 6(b) very small adjustments of L2 had an important influence on the deposition rates. By varying the substrate position a few millimeters from +4.8 mm to −3.2 mm the deposition rate varied from 5.4 to 9.5 μm/h. A further change in substrate position to Zs = −4.9 mm decreased the deposition rate. In this case, the substrate temperature also decreased since the discharge began to separate from the substrate. These experiments demonstrate the need at the higher pressures to vary the coaxial cavity dimensions to achieve optimum, i.e. uniform and high deposition rate, diamond synthesis. These experimental results also support the results of recent plasma modeling [21,22] investigations which indicate that as pressure increases important deposition species concentrations vary considerably within millimeter or less distance and thus suggest that the positioning of the discharge is important in order to obtain optimum synthesis. Thus the reactor tuning adjustments are very useful in order to control and optimize the deposition process.

4. Diamond synthesis results

4.1. Diamond growth rates, morphology and uniformity

A group of experimental deposition runs were performed on one-inch silicon wafers as the pressure was varied from 180 Torr to 240 Torr and methane concentrations were varied from 2% to 5%. Input power levels were changed from 2.1 kW at about 180 Torr to 2.5 kW at 240 Torr as pressure and methane concentrations were varied. For each of these measurements the reactor lengths were adjusted, as indicated in Section 3.3, to yield optimum deposition rates. The growth rates, which are displayed in Fig. 7, increased as the

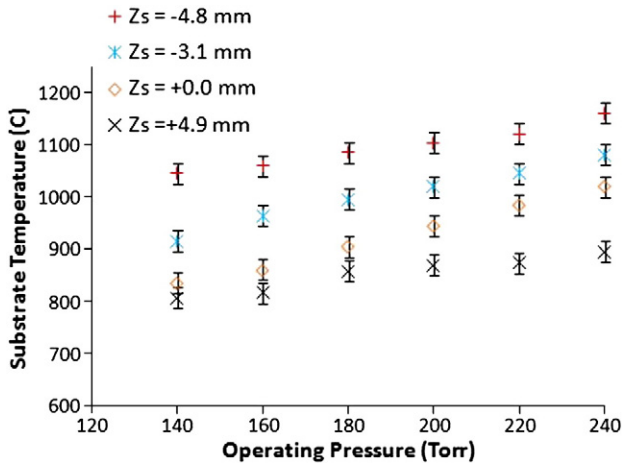

Fig. 5. Substrate temperature with different substrate positions, Zs versus operating pressures.

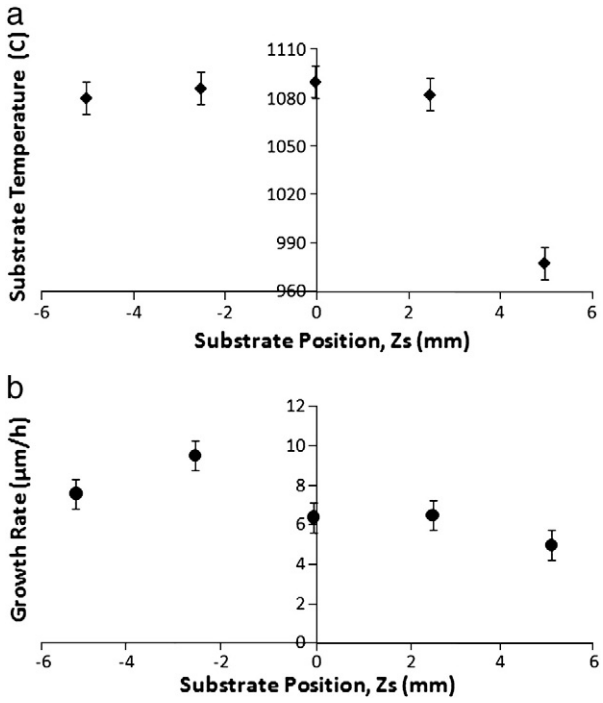

Fig. 6. Substrate temperature (a) and diamond growth rate (b) versus substrate position, Zs. Operating pressure: 220 Torr, CH_4/H_2 concentration: 3%, absorbed power: 2. 4 kW.

operating pressure was increased from 180 to 240 Torr and increased as the methane concentration was increased from 2 to 5%. For all the data points in Fig. 7 the reactor length positions were constant except for a change in Zs. In particular, experiments above 200 Torr, Zs = −0.48 cm and at 200 Torr and below, Zs = −0.31 cm. The PCD growth rates displayed in Fig. 7 are two to three times higher than the growth rates obtained using the reference reactor operating at lower pressures but with similar methane concentration conditions [3,17].

The morphology of the diamond films was observed by analyzing the diamond samples using optical microphotographs as shown in Fig. 8. The Raman spectra of the films were also measured using an argon green laser excitation wavelength of 514.5 nm with spectral width resolution of 0.3 cm^{-1}. Typical examples of the film micro-photographs and associated Raman measurements are shown in Fig. 8. The grown films exhibited morphologies and Raman spectra similar to those reported for thick films grown elsewhere [15,16], and in the reference reactor [3,17] while operating at lower pressure. The Raman spectra were scanned from 1200 to 1800 cm^{-1}. They exhibited a strong sp^3 bonding (diamond) peak at 1332.5 cm^{-1} without sp^2 peaks (G and D bands) between 1500 and 1600 cm^{-1} and the measured full width at half-maximum (FWHM) ranged from 2.5

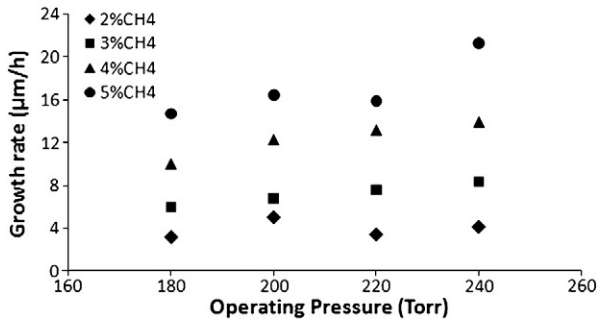

Fig. 7. Diamond growth rate with increasing operating pressure with CH_4 gas chemistries ranging from 2 to 5% with no addition of nitrogen gas into the system.

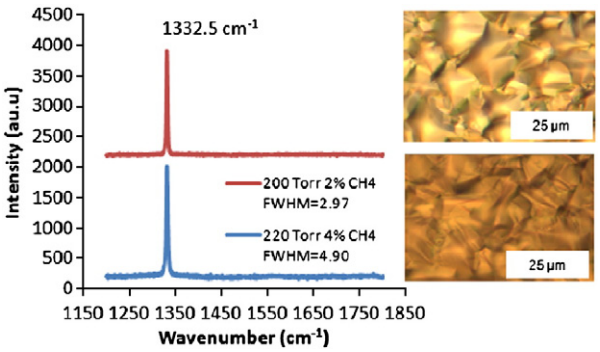

Fig. 8. Raman spectra of polycrystalline diamond grown with Raman peak at 1332.5 cm^{-1} without sp^2 or graphite peak. The right hand side photographs show top surface morphology of polycrystalline diamond films grown at (top) 220 Torr, 4% CH_4, 96 μm thick (bottom) 200 Torr, 3% CH_4, 56 μm thick.

to 9.0 cm^{-1} as the methane concentration was increased from 2% to 5%. In particular, over the 180–240 Torr pressure regime the FWHM varied between 2.5 cm^{-1} and approximately 3.5 cm^{-1} for 2% CH_4/H_2, 3.5 cm^{-1} to 5.5 cm^{-1} for 3% CH_4/H_2, 5.6 to 7.0 cm^{-1} for 4% CH_4/H_2, and 7.0 cm^{-1} to 9.0 cm^{-1} for 5% CH_4/H_2. Thus, the FWHM increased as methane concentration increased. However, for a given constant methane concentration the FWHM did not show a strong definitive pressure dependence i.e., the FWHM was approximately constant versus pressure.

A series of experiments was performed to demonstrate the ability to produce uniform films. The uniformity data for the sample presented in Fig. 9 is the final results of this process. This film had a nominal thicknesses of 73 μm on a 25.4 mm diameter substrate and was grown under the following conditions: (1) operating pressure of 220 Torr, (2) gas flow of 400 sccm H_2 and 12 sccm CH_4, (3) absorbed power of 2.3 kW, (4) substrate temperature of 1120 °C and (5) L1 = 5.65 cm, L2 = 6.05 cm, Ls = 20.3 cm, and Lp = 3.8 cm. Fig. 9 displays the radial and circumferential diamond film uniformity.

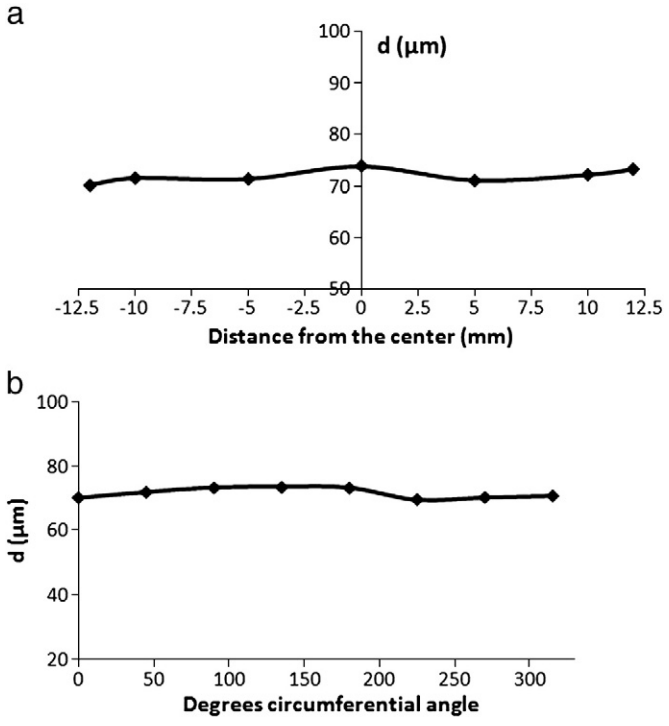

Fig. 9. Diamond film uniformity for a 25.4 mm diameter substrate showing: (a) radial distribution of thickness, d, and (b) circumferential distribution of thickness, d, at a radial distance of 12 mm from the center.

This film was the result of an optimization process that first identified the best cavity lengths (especially L2) that produced relatively uniform (±10–15% thickness percent deviation as discussed in Ref. [17]) films over the one inch silicon substrate. The uniformity was further refined by holding the reactor geometry fixed and slightly varying the input power to produce a plasma discharge that resulted in a very uniform temperature over the substrate.

In Fig. 9, the uniformity is calculated from the diamond thickness profile. The thickness distribution was determined by using a scanning tip connected to a Solarton linear encoder. Prior to diamond deposition, the non-growth surface of the silicon wafer substrate was measured at several points both in radial and circumferential directions. After the deposition, the exact same points on the substrate were re-measured to obtain the final diamond thicknesses. As shown, a good uniformity of grown diamond could be achieved. The variations in the thickness uniformity across the substrate surface were ±1.30 μm radially and ±1.63 μm circumferentially at a radial distance of 12 mm. These variations were determined based on maximum and minimum thickness values across the substrate surface points.

4.2. Diamond quality

Diamond quality was determined from visual observations of the color and transparency of the freestanding films, optical transmission measurements and, as previously noted, Raman spectroscopy. The photograph in Fig. 10 displays a typical freestanding 25 mm diameter 70 μm thick diamond plate deposited at 200 Torr, with 2% methane concentration. After deposition the film was lapped and polished prior to substrate removal via chemical etching. The film exhibits good visual transparency showing the logo underneath the sample. To quantify optical transmission, Fourier transform infrared spectroscopy (FTIR) transmission measurements from 2.5 to 22 μm wavelength were combined with additional spectral measurements from 0.2 to 3.0 μm wavelength. Results are plotted as transmission versus photon energy in Fig. 11. Shown in that figure are the measured transmissions for the 2% methane diamond plate pictured in Fig. 10 and also for a 170 μm thick diamond plate deposited at 220 Torr and 4% methane. At the low energy (long wavelength) portion of Fig. 11, both diamond plates show transmission of approximately 71% as expected for a diamond infrared refractive index of 2.38. The absorption observable for both diamond plates between approximately 25 and 40 meV (3 to 5 μm wavelength) is principally due to two-phonon absorption that occurs in intrinsic diamond. For the 2% methane diamond plate, surface-roughness limited transmission continues throughout the visible and ultraviolet portion of the spectrum until dropping to zero upon the onset of band-gap absorption at 5.5 eV. However the 4% methane window shows optical absorption beginning in the near-infrared and becoming substantial in the visible. The higher methane percentage, higher growth rate, diamond plate may be appropriate for long wavelength applications but the lower methane percentage is required for good performance in the visible and ultraviolet.

Fig. 10. Photograph of free standing diamond film adjacent to a quarter dollar coin after being polished, lapped and silicon substrate removal via chemical etching.

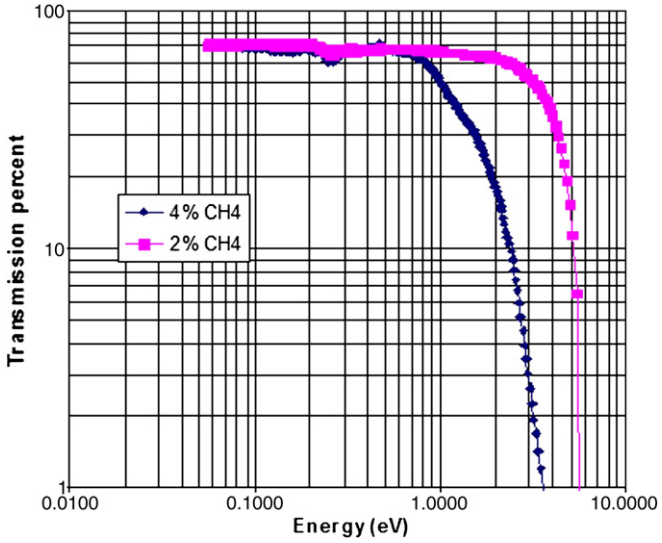

Fig. 11. Transmission spectra for polycrystalline diamond plates grown at 220 Torr at 4% and 200 Torr 2% methane.

5. Summary

A high-pressure and high power density MCPR reactor has been designed and experimentally evaluated by depositing PCD films on one inch silicon substrates over the 180–240 Torr pressure regime. This redesign not only increased the plasma absorbed power density above the substrate but also facilitated operation at higher pressure. The major design changes were (1) the reduction of the inner conductor cooling stage radius by more than a factor of two to 1.91 cm and introducing (2) the position/length tuning of the substrate holder. The reduction of the inner conductor area by 4.5 increased the discharge power density by a factor of 4–5 over the reference design when operating at pressures of 100–150 Torr and produced very intense discharges with adjustable power densities of 150–475 W/cm^3 in the 180–240 Torr pressure regime. The length tuning of the substrate holder allowed the electromagnetic focus to be varied above the substrate and allowed the control of the discharge shape, size and position. The experiments demonstrated that small changes of a few mm in the substrate holder position could change the deposition rate by a factor of two. Also the optimal deposition position varied as pressure and power varied. Thus the length tuning provided an important experimental variable for process control and optimization especially in the high-pressure regime.

Polycrystalline diamond film synthesis rates varied from 3 to 21 μm/h as the operating pressure varied from 180 to 240 Torr and the methane concentration was varied from 2 to 5%. The substrate temperature during the diamond synthesis ranged from 950 to 1150 °C. The diamond growth rate increased with increasing operating pressure and higher methane concentration. These growth rates are two to three times higher than the comparable growth rates of 1–6 μm/h in the lower and moderate pressure, lower power density MCPR [3,17].

Acknowledgement

Matt Swope is thanked for assisting with the Raman instrumentation set up. This research is supported by Fraunhofer USA CCL and the Richard M. Hong Chaired Professorship.

References

[1] T.S. McCauley, Y.K. Vohra, Applied Physics Letters 66 (1995) 1486.
[2] C.-S. Yan, Y.K. Vohra, H.-K. Mao, R.L. Hemley, Proceedings National Academy of Science U. S. A. 99 (2002) 12523.
[3] K.P. Kuo, J. Asmussen, Diamond and Related Materials 6 (1997) 1097.
[4] Y. Mokuno, A. Chayahara, Y. Soda, Y. Horino, N. Fujimori, Diamond and Related Materials 14 (2005) 1743.
[5] A. Tallaire, J. Achard, F. Silva, R.S. Sussmann, A. Gicquel, Diamond and Related Materials 14 (2005) 249.
[6] H. Sternschulte, T. Bauer, M. Schreck, B. Stritzker, Diamond and Related Materials 15 (2006) 542.
[7] H. Yamada, A. Chayahara, Y. Mokuno, S. Shikata, Diamond and Related Materials 16 (2007) 576.
[8] H. Yamada, A. Chayahara, Y. Mokuno, S. Shikata, Diamond and Related Materials 17 (2008) 1062.
[9] H. Yamada, A. Chayahara, Y. Mokuno, Y. Horino, S. Shikata, Diamond and Related Materials 15 (2006) 1383.
[10] H. Yamada, A. Chayahara, Y. Mokuno, Y. Horino, S. Shikata, Diamond Related Materials 15 (2006) 1389.
[11] K.W. Hemawan, T.A. Grotjohn, D.K. Reinhard, J. Asmussen, invited paper presented at International Conference on Plasma Science, session 3E2, Karlsruhe, Germany June (2008).
[12] A.L. Vikharev, A.M. Gorbachev, A.B. Muchnikov, D.B. Radishev, Radiophysics and Quantum Electronics 50 (2007) 913.
[13] A.B. Muchnikov, A.L. Vikharev, A.M. Gorbachev, D.B. Radishev, V.D. Blank, S.A. Terentiev, Diamond and Related Materials 19 (2010) 432.
[14] F. Silva, K. Hassouni, X. Bonin, A. Gicquel, Journal of Physics: Condense Matter 21 (2009) 364202.
[15] A.L. Vikharev, A.M. Gorbachev, A.V. Kolysko, D.B. Radishev, A.B. Muchnikov, Diamond and Related Materials 17 (2008) 1055.
[16] A.L. Vikharev, A.M. Gorbachev, A.V. Kozlov, V.A. Koldanov, A.G. Litvak, N.M. Ovechkin, D.B. Radishev, Yu.V. Bykov, M. Caplan, Diamond and Related Materials 15 (2006) 502.
[17] S.S. Zuo, M.K. Yaran, T.A. Grotjohn, D.K. Reinhard, J. Asmussen, Diamond and Related Materials 17 (2008) 300.
[18] K.P. Kuo, Ph.D. Dissertation, Michigan State University (1997).
[19] U. Kahler, Microwave Plasma Diamond Film Growth, Diplomarbeit Thesis, Michigan State University and Gesamthochschule Wuppertal (1997).
[20] J. Asmussen, D.K. Reinhard, Diamond Films Handbook, Chapter 7, Marcel Dekker Inc., New York, 2002.
[21] Y.A. Mankelevich, P.W. May, Diamond and Related Materials 17 (2008) 1021.
[22] Y.A. Mankelevich, M.N.R. Ashfold, J. Ma, Journal of Applied Physics 104 (2008) 113304.